Applied Catalysis B: Environmental 166–167 (2015) 260–269

Contents lists available at ScienceDirect

Applied Catalysis B: Environmental

journal homepage: www.elsevier.com/locate/apcatb

Effect of Cu substitution on promoted benzene oxidation over porous CuCo-based catalysts derived from layered double hydroxide with resistance of water vapor

Shuangde Li[a], Haosheng Wang[a], Weiman Li[a], Xiaofeng Wu[a], Wenxiang Tang[a,b], Yunfa Chen[a,*]

[a] State Key Laboratory of Multi-phase Complex Systems, Institute of Process Engineering, Chinese Academy of Sciences, Beijing 100190, PR China
[b] University of Chinese Academy of Sciences, Beijing 100049, PR China

ARTICLE INFO

Article history:
Received 27 August 2014
Received in revised form 31 October 2014
Accepted 18 November 2014
Available online 25 November 2014

Keywords:
CuCo-based catalysts
Layered double hydroxide
Catalytic oxidation
Benzene
Water vapor

ABSTRACT

Porous and dispersed CuCo-based mixed metal oxides catalysts (denoted as Cu_xCo_{3-x}Al-MMO) are obtained *via* the calcination of ternary Cu_xCo_{3-x}Al-layered double hydroxide (LDH) precursors, which exhibit excellent catalytic activity towards complete oxidation of benzene. The $Cu_{0.5}Co_{2.5}$Al-MMO sample shows the maximum activity of 2.41 mmol g_{cat}^{-1} h^{-1} with 90% benzene conversion at 290 °C at a high space velocity (SV = 60,000 mL g^{-1} h^{-1}), comparable to that of only 8% conversion for Cu_3Al-MMO sample. The significantly enhanced activity is correlated with higher surface area, narrower pore size, low-temperature reducibility and rich oxygen vacancies and lattice oxygen derived from the synergistic effect over porous and dispersive Cu_xCo_{3-x}Al-MMO catalysts containing CuO and Co_3O_4 spinel mixed oxides verified by XRD, BET, H_2-TPR, TEM and XPS measurements. Stability with prolonged time on benzene stream and the resistance to water vapor are further investigated. In addition, a monolithic CuCoAl-MMO film catalyst is fabricated by an in situ growth-calcination method, which displays comparable catalytic activity with Cu_xCo_{3-x}Al-MMO powder. Therefore, this work provides a facile method for the preparation of CuCo-based catalysts with excellent characters responsible for better catalytic activities, which can be used as promising candidates for practical VOCs oxidation.

1. Introduction

Emission of volatile organic compounds (VOCs) from industrial gases is major contributors to air pollution which may pollute the atmosphere directly or indirectly as secondary pollutants, such as ozone generation and photochemical smog [1–3]. VOCs and their photochemical associated impacts on human health have become a major issue worldwide [4]. The reduction of VOCs is highly desirable and several techniques, e.g. adsorption, high-temperature incineration and catalytic oxidation, have been developed for the abatement of VOCs, of which catalytic oxidation is the most efficient requiring temperatures *ca.* 200–600 °C lower than thermal treatment with above 700 °C [5,6]. The noble metals and transition metal oxides are commonly used for the catalytic oxidation of VOCs. The precious metals (platinum, palladium, etc.) supported on the oxide exhibit higher activity at relatively low temperature, but their high cost, easily sintering and coking, susceptibly poisoning limit their application [7–9]. Transition metal oxides (Fe_2O_3, Cr_2O_3, CuO, Co_3O_4, NiO and MnO_2) as a potential alternative of precious metals, have received much attention for their superior properties such as low cost, high resistance to poisoning, good reducibility [1,3,6,10–12]. Studies reveal that mixed metal oxides own higher catalytic activities than single metal oxide, even equivalent or better than precious metal because of the synergistic effect. Wang demonstrated that a series of MnO_x-CeO_2 mixed oxides catalysts exhibited a much higher activity in the oxidation of benzene than did of the pure MnO_x or CeO_2 because of the much more lattice oxygen playing an important role [13].

Surface area, reducibility and oxygen species are playing a key role in the design and fabrication of highly efficient mixed metal oxides catalysts for total VOCs oxidation. A large number of catalysts have been designed to improve the above properties. Ordered cobalt oxides employed by a nanocasting route or template method exhibited the enhanced catalytic activity for propane and toluene decomposition in terms of both the high surface area and the presence of oxygen vacancies [6]. Li reported binary Cu-Co catalysts

* Corresponding author. Tel.: +86 10 8254 4896; fax: +86 10 8254 4896.
E-mail addresses: chenyf@ipe.ac.cn, yfchen@ipe.ac.cn (Y. Chen).

http://dx.doi.org/10.1016/j.apcatb.2014.11.040
0926-3373/

derived from hydrotalcites with excellent activity and recyclability towards NH_3BH_3 dehydrogenation for the highly dispersed Cu and Co_3O_4 species facilitates the low temperature reducibility [14]. Oxygen mobility and reactivity of lattice oxygen can be enhanced by the oxygen vacancies existing on the catalysts, which are proved beneficial for toluene combustion over manganese oxide catalysts [15,16]. Despite all this progress, a huge challenge still remains to achieve high active VOCs catalysts possessing at least some or all the excellent properties with higher surface area, low temperature reducibility and rich lattice oxygen species simultaneously.

Layered double hydroxides (LDH) are a class of naturally occurring and synthetic materials generally expressed by the formula $[M^{2+}_{1-x}M^{3+}_{x}(OH)_2](A^{n-})_{x/n} \cdot mH_2O$, in which M^{II} and M^{III} cations disperse in an ordered and uniform manner in brucite-like layers, and A^{n-} is a charge compensating anion such as NO_3^-,·CO_3^{2-}, metal complexes, surfactant or other ligands [17–20]. The cation composition of LDH-related mixed oxide catalysts can be simply adjusted during precursor synthesis [21]. After heating at moderate temperatures, the resulting mixed oxides catalysts from a topotactic transformation of LDH give finely dispersed mixed oxides of M^{II} and M^{III} metals with a sufficiently large surface area and good thermal stability [22–25]. Furthermore, the synergistic effect due to the good interspersion of the oxide phases would possess some desirable features, like low temperature reducibility and more lattice oxygen for the improvement of catalytic activity. Besides, the presence of LDH matrix inhibits the agglomeration of active components and thus enhances the long-term stability.

Development of efficient and durable catalysts for VOCs degradation has been one of the most active research areas. In the well-studied transition metals, cobalt (Co) and copper (Cu) are very efficient catalysts towards VOCs oxidation. In this work, we report the fabrication of Cu_xCo_{3-x}Al-MMO powdered mixed metal oxide catalysts via a facile two-step procedure involving preparation of a ternary Cu_xCo_{3-x}Al-LDH precursor followed by a calcination process. Note that benzene can be produced from diverse sources, e.g. from printing and petrochemical industries and it can increase the risk of cancer and other illnesses, even leukemia for long-term exposure to excessive level of benzene. Benzene is therefore chosen to assess the catalytic activity over the as-prepared catalysts. The aim of the present study is to investigate systematically the effect of Cu (or Co) substitute on the nature of the texture properties of surface area, redox, oxygen species and catalytic activities of Cu_xCo_{3-x}Al-MMO catalysts. The $Cu_{0.5}Co_{2.5}$Al-MMO sample yields largely enhanced catalytic activity with T90 for benzene conversion at 290 °C at a high space velocity (SV = 60,000 mL g^{-1} h^{-1}). XRD, H_2-TPR, HRTEM and XPS measurements demonstrate that the $Cu_{0.5}Co_{2.5}$Al-MMO sample possesses the larger surface area, the smaller pore size, the low temperature reducibility and the most ratio of lattice oxygen to adsorbed oxygen, because the interspersion between CuO and Co_3O_4 nanoparticles maximizes the synergistic effect, accounting for the significantly enhanced activity. The $Cu_{0.5}Co_{2.5}$Al-MMO catalysts were further investigated to display long stability with prolonged time on benzene stream and the resistance to water vapor. Moreover, we have successfully fabricated a monolithic highly dispersed CuCoAl-MMO film catalyst by an in situ growth-calcination method, which exhibits comparable catalytic activity with Cu_xCo_{3-x}Al-MMO powder.

2. Experimental

2.1. Cu_xCo_{3-x}Al-MMO catalysts powder preparation

All chemicals used in this study were commercially available (from Merck) and used without further purification. Pure aluminum substrate (purity >99.99%; thickness 0.2 mm) was purchased from Beijing General Research Institute. To assess the effect of Cu^{2+}(or Co^{2+}) on the properties of Cu_xCo_{3-x}Al-MMO catalysts, seven LDHs precursors samples by varying the concentration of the two metal ions mixed nitrate salt solutions of Cu^{2+} and Co^{2+} (with Cu:Co molar ratios of 0:3, 0.5:2.5, 1:2, 1.5:1.5, 2:1, 2.5:0.5, 3:0 and $(Cu^{2+} + Co^{2+})/Al^{3+}$ molar ratio of 3:1) were prepared by a co-precipitation method (denoted as Cu_xCo_{3-x}Al-LDH, where x stands for the nominal Cu substitution). The preparation procedure was dropwised 1 M, 20 mL mixed salt solution of divalent ($Cu(NO_3)_2{\cdot}3H_2O$) and $Co(NO_3)_2{\cdot}6H_2O$) and trivalent ($Al(NO_3)_3{\cdot}9H_2O$) and 1.5 M, 30 mL NaOH solution at the same time to a 0.056 M, 180 mL Na_2CO_3 solution keeping at constant pH 9.5 at 65 °C with constant stirring for 18 h. The resulting suspension was centrifuged with deionized water, and then dried at 80 °C for overnight. The catalysts of Cu_xCo_{3-x}Al-MMO were obtained by calcinating the products of Cu_xCo_{3-x}Al-LDH precursors in air at 400 °C for 4 h with a heating rate of 10 °C min^{-1} (denoted as Cu_xCo_{3-x}Al-MMO).

2.2. Monolithic CuCoAl-MMO film catalyst preparation

The CuCoAl-LDH film was prepared by in situ crystallization on pure aluminum substrate (99.99%), which was cleaned with acetone, ethanol and deionized water in sequence before use. In a typical procedure, $Cu(NO_3)_2{\cdot}3H_2O$ (5 mmol), $Co(NO_3)_2{\cdot}6H_2O$ (5 mmol) and $(NH_2)_2CO$ (60 mmol) were dissolved in 300 mL deionized water to form a clear solution. The Al substrate (4 × 15 cm) was rolled into a tubular shape and immersed vertically in the solution, which was heated at 70 °C for 30 h, then CuCoAl-LDH film was grown along their *ab*-orientation vertical to Al substrate. Afterwards, the substrate was withdrawn, rinsed with deionized water and dried at room temperature. Then the as-prepared CuCoAl-LDH film was heated at 400 °C for 4 h with 10 K min^{-1} in muffle, and cooled to room temperature to obtain the CuCoAl-MMO film. The Al substrate grown with CuCoAl-LDH film and CuCoAl-MMO film was measured by XRD and SEM.

2.3. Characterization of the catalysts

X-ray diffraction (XRD) patterns of the catalysts were measured on a Rikagu SmartLab system using Cu Kα radiation in the diffraction angle (2θ) range 8–90°. The specific surface areas and pore size distributions of all catalysts were obtained according to the Brunauer–Emmett–Teller (BET) and Barrett–Joyner–Halenda (BJH) methods, respectively, using the N_2 adsorption–desorption method on an automatic surface analyser (AS-1-C TCD, Quantachrome Cor., USA) at 77 K. Before measurement, each sample was degassed at 200 °C for 3 h. The samples morphology was recorded on a scanning electron microscope (SEM, JEOL JSM-6700F, Japan, 15 kV, 10 mA). The microstructures of samples were obtained using transmission electron microscopy (TEM, JEOL JEM-2010F) with an accelerating voltage of 200 kV. Surface species of the as-prepared catalysts were determined by X-ray photoelectron spectroscopy (XPS) and X-ray induced Auger electron spectroscopy (XAES) using a XLESCALAB 250Xi electron spectrometer from VG Scientific with monochromatic Al K*a* radiation (1486.6 eV). Hydrogen temperature programmed reduction (H_2-TPR) with 30 mg catalyst (40–60 mesh) was carried out in an U-shaped quartz reactor under a gas flow (5% H_2 balanced with Ar, 25 mL min^{-1}). In each procedure, the temperature was raised to 800 °C from room temperature at a constant rate of 10 °C min^{-1}.

2.4. Catalytic activity tests

Performance of catalysts was evaluated in a continuous-fixed-bed quartz microreactor (i.d. 6 mm) at a space velocity (SV) of

Table 1
Lattice parameters and atomic ratio for different $Cu_xCo_{3-x}Al$-LDH.

LDH	*a* (Å)	*c* (Å)	Intial Cu:Co atomic ratio	Cu:Co atomic ratio from SEM-EDX	XPS
Co_3Al	3.08	22.83	–	–	
$Cu_{0.5}Co_{2.5}Al$	3.07	22.77	0.2	0.28	0.25
Cu_1Co_2Al	3.07	22.60	0.5	0.47	
$Cu_{1.5}Co_{1.5}Al$	3.06	22.57	1	1.25	
Cu_2Co_1Al	3.07	22.50	2	2.87	1.34
$Cu_{2.5}Co_{0.5}Al$	–	22.21	5	4.85	
Cu_3Al	–	21.77	–	–	

60,000 mL g^{-1} h^{-1}. The temperature of the reactor was controlled using a temperature controller. Catalysts (100 mg, 40–60 mesh) were loaded in the quartz reactor with quartz wool packed at both ends of the catalyst bed. 1000 ppm benzene balanced with air was purged into the reactor at a continuous flow 100 mL min^{-1} using mass flow controllers. For the consideration of water vapour's effect, the mixed gas composed of a relative 1.5% water vapour and 500 ppm benzene generated by mixing an 50 mL min^{-1} air flow used for bubbling water and 50 mL min^{-1} another air flow with benzene, was purged into the reactor for catalytic tests. The concentration of benzene in the effluent gas was analysed by a gas chromatograph (Shimadzu GC-2014) equipped with a flame ionization detector (FID) and the concentration of CO_2 in the outlet gas was detected by another FID with a methanizer furnace for converting CO_2 to CH_4. The catalytic evaluation for CuCoAl-MMO film catalyst on the Al substrate was performed by replacing CuCoAl-MMO powder samples with film catalyst which was pre-tailored to very small fragments. The complete conversion of benzene ($W_{benzene}$) and the yield of CO_2 (η_{CO_2}) were calculated as follows:

$$W_{benzene} = \frac{C_{benzene,in} - C_{benzene,out}}{C_{benzene,in}} \times 100\%.$$

$$\eta_{CO_2} = \frac{C_{CO_2,out}}{6 \times C_{benzene,in}} \times 100\%.$$

where $C_{benzene,in}$ (ppm), $C_{benzene,out}$ (ppm) and $C_{CO_2,out}$ (ppm) are the concentrations of benzene in the inlet and outlet gas, and CO_2 in the outlet gas, respectively.

3. Results and discussion

3.1. Textural study of the catalysts

The XRD patterns of $Cu_xCo_{3-x}Al$-LDH precursors with increasing Cu:Co molar ratios from 0 to 5 are shown in Fig. 1A. In each case, the XRD pattern exhibits the characteristic reflections of LDH materials with a series of (0 0 *l*) peaks appearing as narrow symmetric lines at a low angle with 3R packing of layers. The lattice parameter $a = 2d(1\,1\,0)$ around $2\theta = 60°$,which is coincides with the closest M–M distance within the layers, while $c = 3d(0\,0\,3)$ around $2\theta = 11.6°$, which is as a function of the interlayer distance. They are calculated and summarized in Table 1. It appears that the lattice parameter *a* and *c* decreases with increasing Cu^{2+} substitution in the brucite layer (in Fig. 1A, inset and Table 1), possessing different ionic radius with the larger one of Co^{2+} (0.74 Å) and smaller one of Cu^{2+} (0.69 Å) in an octahedral environment [26,27]. It should be noticed that the two peaks of (1 1 0) and (1 1 3) reflections around $2\theta = 60°$ and 61° decrease both in intensity and sharpness with increased Cu content especially from Cu-rich sample $Cu_{2.5}Co_{0.5}Al$-LDH to Cu_3Al-LDH, for the respect of the Jahn–Teller distortion of Cu^{2+} (d^9 configuration) ion, leading to poor long-range ordering, commonly reported for copper divalent LDH systems, CuCoCr-LDH or Cu_2Cr-LDH [27,28]. Furthermore, the broadening of diffraction lines in the $Cu_xCo_{3-x}Al$ LDH patterns with increased Cu content, especially *d*(0 0 3) line is probably attributed to both crystallite size effects and structural disorder [29].

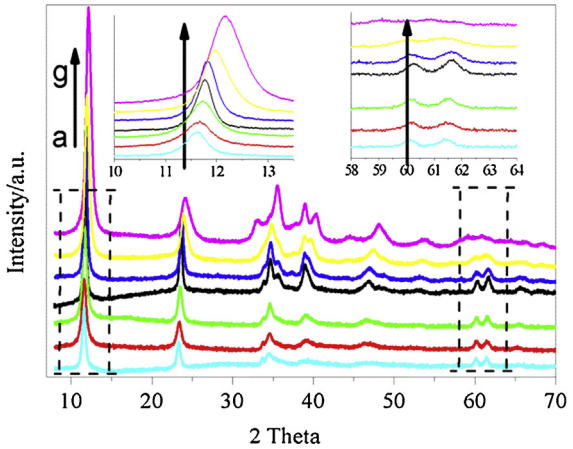

Fig. 1. (a–g) XRD patterns of Co_3Al, $Cu_{0.5}Co_{2.5}Al$, Cu_1Co_2Al, $Cu_{1.5}Co_{1.5}Al$, Cu_2Co_1Al, $Cu_{2.5}Co_{0.5}Al$, Cu_3Al-LDH precursors. The insets are the zooming image.

The morphology of $Cu_xCo_{3-x}Al$-LDH revealed by SEM is shown in Fig. 2. $Cu_xCo_{3-x}Al$-LDH show uniform and randomly oriented hexagonal lamellar structure. The particle size decreased from *ca.* 260 nm for $Cu_{0.5}Co_{2.5}Al$-LDH to *ca.* 80 nm for Cu_2Co_1Al-LDH, which is coincided with the gradual broader XRD peak at $2\theta = 11.6°$ with enhanced Cu content [29]. Besides, for Cu-rich samples, like Cu_2Co_1Al-LDH, the edge of the hexagonal lamellar structure turns to obscure, close to filmy sphere, which may be leading the reduction of surface area. The Cu/Co ratios in the LDH detected from SEM-EDX summarized in Table 1 were reasonably coincident with the ratios in the initial solutions with small deviation, which is rather commonly observed in LDH preparation with co-precipitation method [18].

After calcination in air at 400 °C, the $Cu_xCo_{3-x}Al$-LDH transform to a mixture of oxide and spinel phase detected from XRD diffraction of $Cu_xCo_{3-x}Al$-MMO catalysts given in Fig. 3. Diffraction reflections at $2\theta = 35.5$ and 38.8 indicate the formation of CuO phase in Fig. 3g (PDF card No. 65–2309). The strongest reflection at $2\theta = 36.8$ correspond to a Co_3O_4 spinel phase in Fig. 3a (PDF card No. 34-0425). As the copper content is increased, the intensities of the Co_3O_4 peaks decrease and the peaks become broader, and two maxima for CuO phase develop and their intensities increase. The existence of such mixed oxide phase containing both CuO and Co_3O_4 spinel phases is expected to bring about an interaction between them, which would alter the physicochemical properties of the catalysts and is expected to advance the catalytic activities. Furthermore, the amorphous Al_2O_3 matrix in MMO can play a role of support to stabilize and disperse the CuO and Co_3O_4 spinel phases, which are also favorable to high catalytic activity. They have a rising dispersion and immobilization for being grafted within an amorphous Al_2O_3 matrix with strong interaction, and located in different layers hard to migrate over the interlayer spaces, since agglomeration is effectively inhibited [30–32]. The TEM images of the $Cu_xCo_{3-x}Al$-MMO catalysts shown in Fig. 4 maintain the

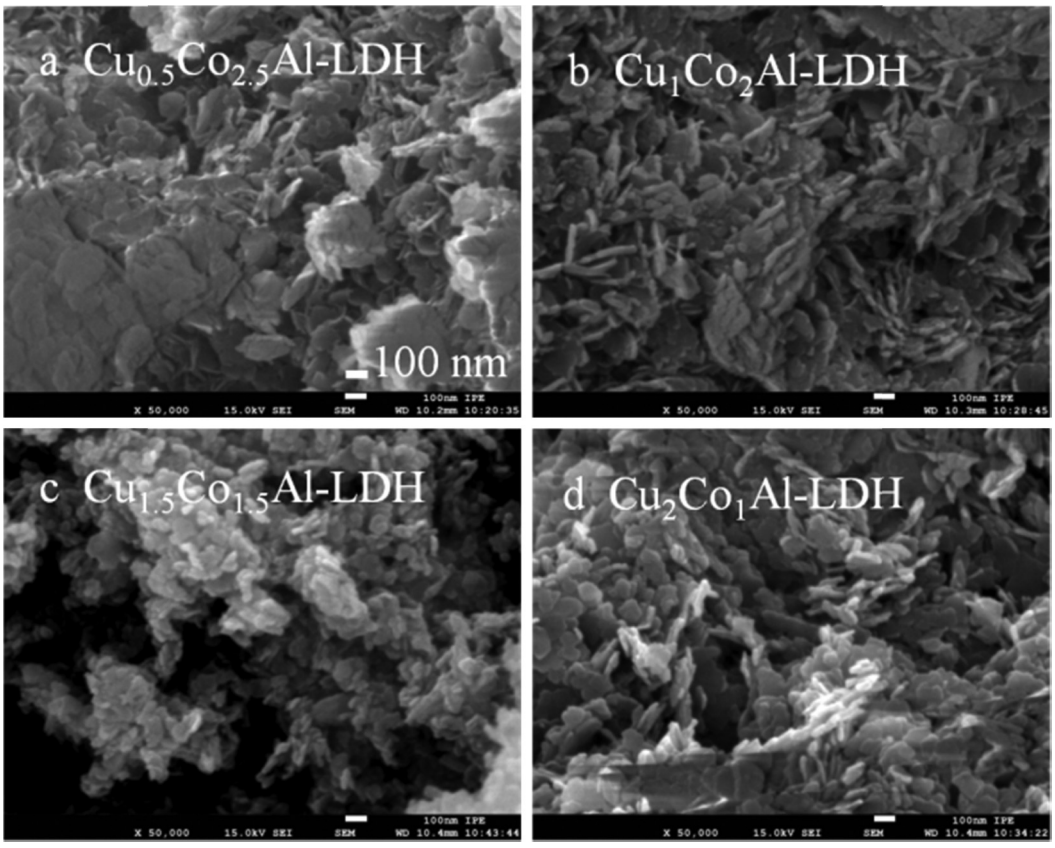

Fig. 2. (a–d) SEM of $Cu_{0.5}Co_{2.5}Al$, Cu_1Co_2Al, $Cu_{1.5}Co_{1.5}Al$ and Cu_2Co_1Al-LDH.

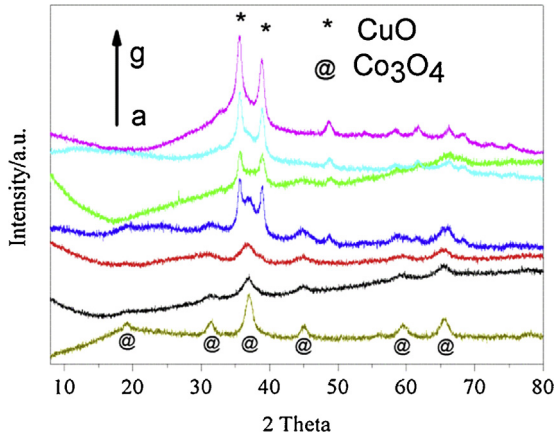

Fig. 3. (a–g) XRD patterns of Co_3Al-MMO, $Cu_{0.5}Co_{2.5}Al$-MMO, Cu_1Co_2Al-MMO, $Cu_{1.5}Co_{1.5}Al$-MMO, Cu_2Co_1Al-MMO, $Cu_{2.5}Co_{0.5}Al$-MMO, Cu_3Al-MMO samples.

plate-like morphology of the original LDH precursor. Additionally, Co_3Al-MMO, Cu_2Co_1Al-MMO and Co_3Al-MMO samples in Fig. 4a, c and e all present pore embedded in the plate matrix. The pore is around 2.5 nm for Co_3Al-MMO sample, which facilitates catalysis by augmenting contact between reactant and catalysts. The structure of $Cu_xCo_{3-x}Al$-MMO catalysts is revealed by HRTEM (Fig. 4b, d and f). Two identified fringes with lattice spacing of 0.23 and 0.25 nm are indexed to the (2 2 0) plane of Co_3O_4 spinel phase with well crystallization and (1 1 1) plane of CuO phase with little poor crystallization, respectively. This observation is in agreement with the XRD results. TEM show $Cu_xCo_{3-x}Al$-MMO catalysts are porous and the CuO and Co_3O_4 species are dispersed.

Fig. 5 displays the N_2 adsorption–desorption isotherm and the corresponding pore size distribution curve for the $Cu_xCo_{3-x}Al$-MMO catalysts. All the samples exhibit a typical IV isotherm with a H3-type hysteresis loop ($P/P_0 > 0.4$), indicating the presence of mesoporous, which are further confirmed by the distribution of pore size (Fig. 5B). This is commonly observed with aggregates of plate like particles of LDHs precursor which remained in the calcined mixture, giving rise to slit-shaped pores [33,34]. The samples show a gradually decreased specific surface area from 153.5 to 32.1 $m^2\ g^{-1}$ and increased pore size from 3.37 to 44.76 nm, and little variation of pore volume around 0.22–0.35 $cm^3\ g^{-1}$ as the enhanced Cu content (Table 2), which will be beneficial for the disparity of the catalytic activity.

3.2. Evaluation of the catalytic behavior

The catalytic performances of $Cu_xCo_{3-x}Al$-MMO catalysts were evaluated in the oxidation of benzene as a function of the temperature, 150–400 °C shown in Fig. 6. The temperatures of 10% (T10), 50% (T50), and 90% (T90) benzene conversion are summarized in Table 2. Upon addition little of Cu to Co_3Al-MMO, the activity increases firstly, when the Cu content continuously increases, the catalytic activity starts to decrease, even worse than that of Co_3Al-MMO, which indicates $Cu_{0.5}Co_{2.5}Al$-MMO is the most active among all catalysts achieving complete benzene conversion at 315 °C. The reaction rate for benzene oxidation at T90 = 290 °C on $Cu_{0.5}Co_{2.5}Al$-MMO is about 2.41 mmol $g_{cat}^{-1}\ h^{-1}$ which is clearly greater than that on Co_3Al-MMO catalyst with 2.06 mmol $g_{cat}^{-1}\ h^{-1}$ and on Cu_3Al-MMO catalyst with 0.27 mmol $g_{cat}^{-1}\ h^{-1}$. The excellent activity on the $Cu_{0.5}Co_{2.5}Al$-MMO can be attributed to the high surface area and small pore size, the rich lattice oxygen species and the good low temperature reducibility developed from synergistic effect. This

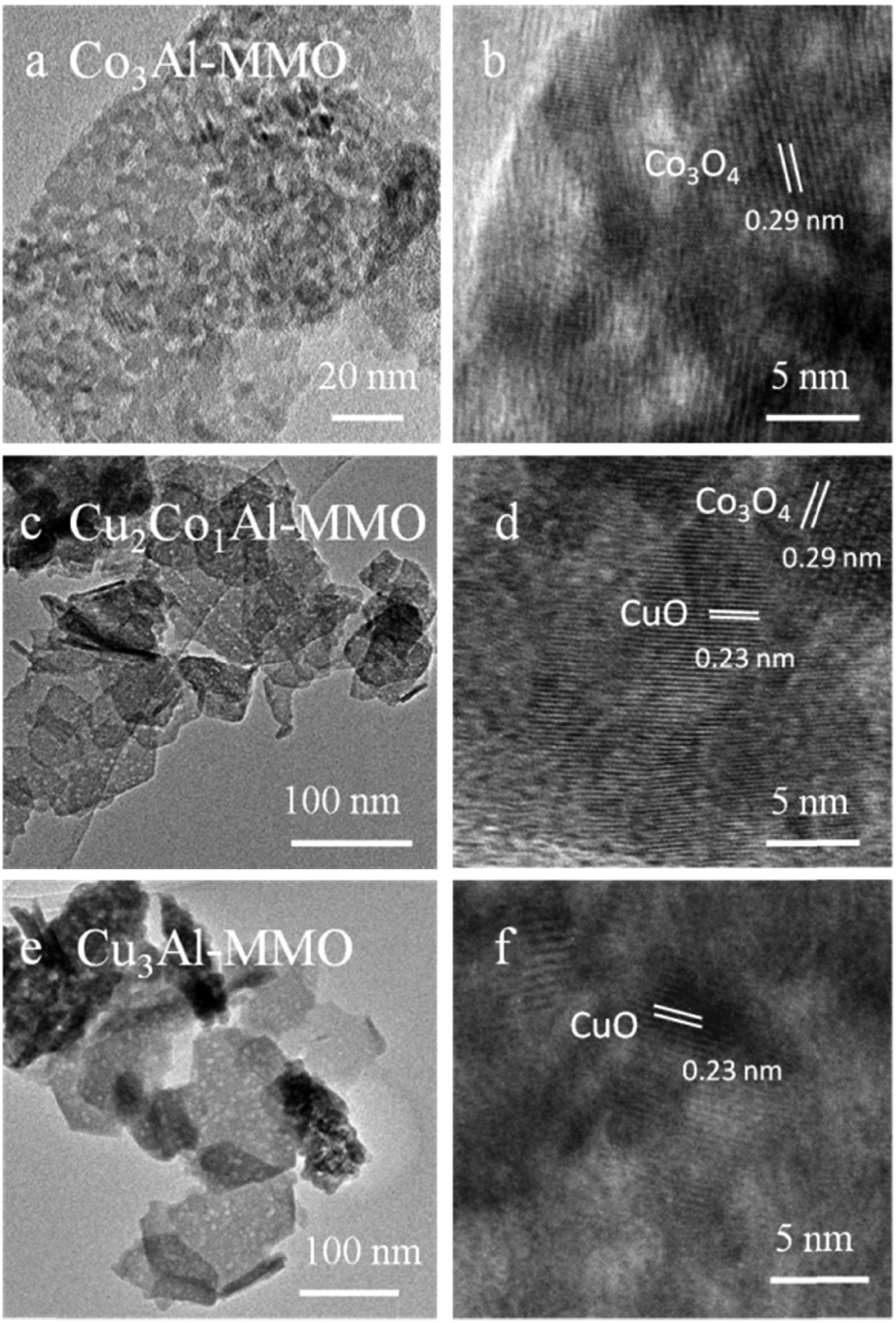

Fig. 4. (a, c, e) TEM images of the catalysts, Co_3Al-MMO, Cu_2Co_1Al-MMO and Cu_3Al-MMO. (b, d, f) The corresponding HRTEM images in a, c and e, respectively.

illustration will be researched in the following text. The activities of some Cu/Co-based catalysts reported in other literatures [35–38] for benzene oxidation for T90 conversion are listed in Table 3. As we can see, most catalysts in other reports have poor activity for T90 benzene conversion beyond 300 °C and few catalysts have better activity around 250 °C with quite low benzene concentration. And the T90 conversion on our materials is about 290 °C with higher SV at 60,000 mL g^{-1} h^{-1} which is clearly greater than others.

The evolutions of time-on-stream of benzene conversion at 310 °C for the $Cu_{0.5}Co_{2.5}Al$-MMO catalyst and the effect of water vapor are shown in Fig. 6B. The catalytic activity was not significant drop in benzene conversion from 94.5% to 93.8% over 10 h of running. In the following 14 h stream of benzene with the presence of 1.5% water vapor, it can be seen that water vapor had a little negative effect on the catalyst, leading the benzene conversion from 93.8% to 91.7%. This was attributed to water vapor may cover some

Table 2
Physical characterization, catalytic activities and surface elemental ratio of Cu, Co and O 1 s from XPS.

LDH	BET surface areas ($m^2\ g^{-1}$)	Pore volume ($cm^3\ g^{-1}$)	Pore size (nm)	Benzene conversion			Co^{2+}/Co^{3+} molar ratio	O_{latt}	O_{ads}	O_{latt}/O_{ads}
				T10	T50	T90				
Co_3Al-MMO	153.5	0.34	3.37	230	268	304	0.47	0.54	0.31	1.74
$Cu_{0.5}Co_{2.5}Al$-MMO	127.2	0.23	9.58	214	250	290	0.59	0.48	0.24	2.00
Cu_1Co_2Al-MMO	112.9	0.24	9.69	220	259	304				
$Cu_{1.5}Co_{1.5}Al$-MMO	83.2	0.25	16.91	228	275	335				
Cu_2Co_1Al-MMO	54.1	0.22	17.32	245	300	354	0.52	0.32	0.68	0.47
$Cu_{2.5}Co_{0.5}Al$-MMO	52.0	0.35	16.72	260	314	356				
Cu_3Al-MMO	32.1	0.25	44.76	290	–	–		0.15	0.85	0.18

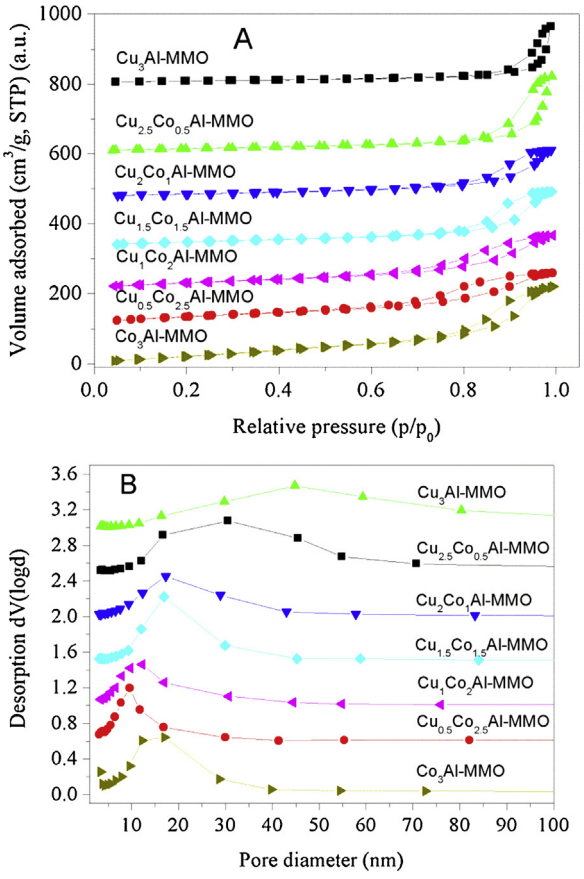

Fig. 5. (A) N_2 adsorption–desorption isotherms curves and (B) pore size distributions calculated from the desorption branch of as-synthesized $Cu_xCo_{3-x}Al$-MMO catalysts.

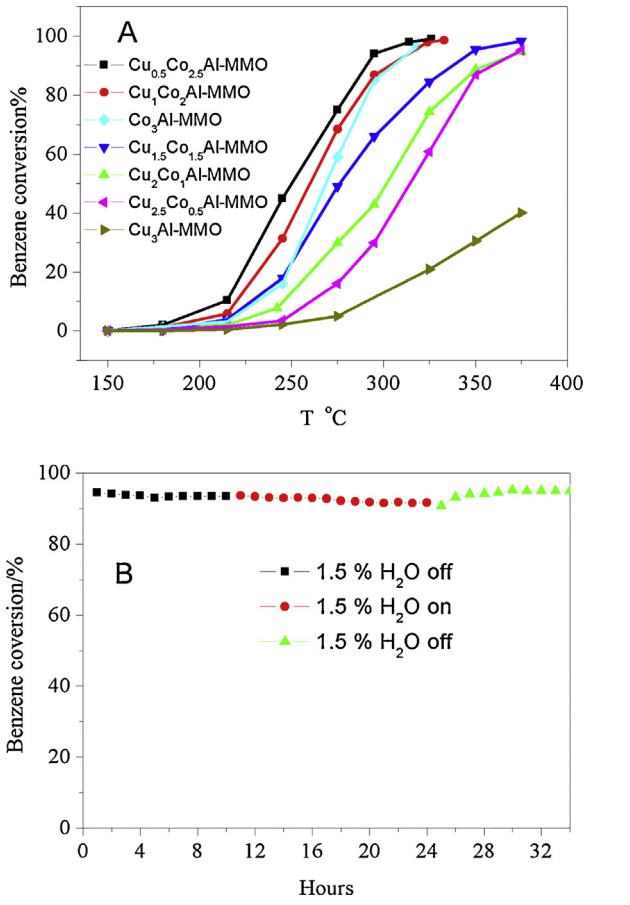

Fig. 6. (A) Benzene conversion as a function of reaction temperature over $Cu_xCo_{3-x}Al$-MMO catalysts under the conditions of benzene concentration 1000 ppm in air, SV = 60,000 mL g^{-1} h^{-1}; (B) the effect of 1.5% water vapor mixed in the stream with 500 ppm benzene over $Cu_{0.5}Co_{2.5}Al$-MMO catalyst, SV = 60,000 mL g^{-1} h^{-1} at 320 °C for 34 h with and lack of water vapor.

active sites which are available for the reaction competed with benzene molecules or oxygen molecules leading to a reduction of the number of the active sites [39,40]. Luckily, after removing water vapor, the benzene conversion refreshed and maintained to 94.5%

Table 3
Main data of research papers on benzene oxidation over Cu and Co related oxide catalysts.

Catalysts	Surface area ($cm^3\ g^{-1}$)	VOC concentration (ppm)	SV (mL g^{-1} h^{-1})	Conversion of T90 (°C)	Ref.
Cu/SBA-16		1000	20,000	420	[35]
Co/SBA-16	347	1000	20,000	320	[35]
CoCe(18:1)/SBA-16	332	1000	20,000	260	[35]
CoCe(18:1)/SBA-16	332	1000	80,000	300	[35]
$CuCo/Al_2O_3$		49		250 (T99)	[36]
$5.5\%Cu/Al_2O_3$		10,000	30,000	350	[37]
$5.5\%Cu/TiO_2$		10,000	30,000	250	[37]
Co/Al-PILC		130–160	20,000	370	[38]
Cu/Al-PILC		130–160	20,000	500	[38]
$Cu_{0.5}Co_{2.5}AlO$	127	1000	60,000	290	Our work

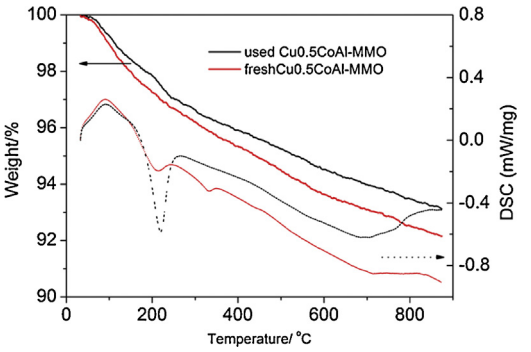

Fig. 7. TG and DSC curves for used after 24 h catalytic reaction at 290 °C and fresh $Cu_{0.5}Co_{2.5}Al$-MMO catalysts under synthetic air.

with the following 10 h benzene stream, which manifested that the $Cu_{0.5}Co_{2.5}Al$-MMO catalyst can stand up to the water vapor and keep the excellent catalytic activities under certain extent.

The yield of CO_2 was also detected and calculated to evaluate if benzene was completely oxidized to CO_2 and H_2O over $Cu_xCo_{3-x}Al$-MMO catalysts. Unfortunately, the yields of CO_2 are a little deviation 3–5% compared with benzene conversion over all the $Cu_xCo_{3-x}Al$-MMO catalysts from 150 to 380 °C, which may due to the error caused by the CO_2 monitoring method through converting CO_2 to CH_4 with a methanizer furnace, or little by-products absence of detection in our experimental process. The complete benzene conversion with no other by-products detected in our system maybe due to catalytic oxidation are under rich O_2 condition, both the lattice oxygen and adsorbed oxygen species, like O^{2-}, O_2^- or O^- will promote total oxidation to CO_2 and H_2O quickly on the interface of catalyst [41], commonly reported in other VOCs catalytic oxidation over mixed metal oxides catalysis [40].

To evaluate the coke deposition leading catalytic deactivation over benzene oxidation, the TG/DSC experiments under synthetic air over used (after 24 h catalytic reaction at 290 °C) and fresh $Cu_{0.5}Co_{2.5}Al$-MMO catalysts are performed shown in Fig. 7. It is known that deposited carbon on catalysts has different morphologies and structures with different oxidation temperatures, usually has an obvious exothermic peak centered around 500 °C within 400–800 °C related to the burning of easy to eliminate carbon species together with clear weight loss, like filamentous structures [42]. The DSC curve in Fig. 7 shows one endothermic peak and one exothermic peak, with approximate onset temperatures of 100 and 215 °C, respectively, corresponds to the loss of water and volatile materials adsorbed on the surface [42]. There are no obvious DSC exothermal peaks between 400 and 800 °C and the used catalyst possessed less weight loss than fresh catalyst, which manifested free of carbon deposition on benzene catalytic oxidation over $Cu_xCo_{3-x}Al$-MMO. This is because carbon deposition are easily happened on partial oxidation with less O_2 existence [42], but under enough O_2 existence leading to deep oxidation, coking is less happened [40].

3.3. X-ray photoelectron spectra

To obtain further insights into the structure–function correlations, X-ray photoelectron spectra (XPS) were obtained for the fresh samples of Co_3Al-MMO, $Cu_{0.5}Co_{2.5}Al$-MMO, Cu_2Co_1Al-MMO and Co_3Al-MMO catalysts. The survey spectra for Cu 2p, Co 2p, and O 1s are displayed in Fig. 8, all of which are referenced to the residual carbon at a binding energy (BE) of 284.6 eV. For the sample of fresh $Cu_{0.5}Co_{2.5}Al$-MMO, Cu_2Co_1Al-MMO and Cu_3Al-MMO, the peaks at 934.2 and 954.1 eV (Fig. 8A) are attributed to Cu $2p_{3/2}$ and Cu $2p_{1/2}$, respectively, with satellite peaks observed at 942.5 and 963.0 eV, corresponding to a Cu^{2+} state with a d9 electron configuration [43]. It should be noticed that another weak Cu 2p peak at 931.6 eV is observed only for $Cu_{0.5}Co_{2.5}Al$-MMO sample, which may be ascribed to the generation of Cu^+ species probably responsible for the remarkable catalytic activity [40]. To confirm the Cu^+ species, XAES for Cu LMM in $Cu_{0.5}Co_{2.5}Al$-MMO and Cu_1Co_2Al-MMO samples were recorded shown in Fig. 8D, which is good at distinguishing Cu^+ and Cu^{2+} [44]. However, there is only one peak maximum at a kinetic energy of the Cu LMM transition at 917.8 eV belong to CuO, in agreement with literature values [44]. This can confirm that the highest activity of $Cu_{0.5}Co_{2.5}Al$-MMO sample is independent of Cu^+, but bring about the characters derived from the synergistic effect.

Two broad and asymmetric peaks located around 780 and 796 eV (Fig. 8B) correspond to Co $2p_{3/2}$ and Co $2p_{1/2}$ from the spin–orbit doublet of Co_3O_4, respectively, suggesting composed by two nonresolved components originated by Co^{2+} and Co^{3+} states [45]. The Co 2p spectra is adopted to decompose for allowing the assignment of Co oxides states. The predominant peak at 780.4 eV and a small peak at 781.8 eV are attributed to Co^{3+} and Co^{2+} $2p_{3/2}$ configuration. The Co^{3+} and Co^{2+} $2p_{1/2}$ components appear at 795.5 and 797.5 eV [6]. The weak shake-up satellite structure appears at 787 eV higher in energy than the main Co 2p3/2 doublet assigned to the Co^{2+} state. Co $2p_{3/2\text{-}1/2}$ splitting within 15 eV agrees with those in the literature [46]. The surface area ratio of the Co $2p_{3/2}$ peaks of Co^{2+} and Co^{3+} is 0.47, 0.59, 0.52 eV, respectively, for Co_3Al-MMO, $Cu_{0.5}Co_{2.5}Al$-MMO and Cu_2Co_1Al-MMO samples, all around 0.5, corresponds to the formula $Co^{2+}(Co^{3+})_2O_4$ [46]. The $Cu_{0.5}Co_{2.5}Al$-MMO sample presents a higher concentration of surface Co^{2+}, which could be an indication of oxygen vacancies close to surface [47], corresponding to the higher intrinsic catalytic activity. XPS results further confirmed the presence of CuO and Co_3O_4 spinel in the $Cu_xCo_{3-x}Al$-MMO catalysts.

The asymmetric O 1s peaks for $Cu_xCo_{3-x}Al$-MMO samples can be deconvoluted into two or three contributions centered at 530, 531 and 533 eV, which are attributed to the lattice oxygen (O_{latt}), surface adsorbed oxygen (O_{ads}) and surface oxygen of hydroxyl species or adsorbed water species, respectively [13,48]. Surface molar percent of O_{latt}, O_{ads} and $O_{latt/Oads}$ are summarized in Table 2. The $O_{latt/Oads}$ molar ratio firstly increases from 1.74 for Co_3Al-MMO to 2.00 for $Cu_{0.5}Co_{2.5}Al$-MMO with the addition of Cu, then drastically decreases to 0.47 for Cu_2Co_1Al-MMO and 0.18 for Cu_3Al-MMO (Table 2), implying that one can enrich the surface lattice oxygen of $Cu_xCo_{3-x}Al$-MMO catalysts by incorporating a little Cu. They may be due to the higher surface specific area and narrower pore size creates more vacancies and unsaturated chemical bonds, which will lead to the increase of lattice oxygen ratio on the surface. The sequence of O_{latt}/O_{ads} molar ratio is identical with that of benzene catalytic oxidation activity. It is noticeable that the distribution of surface species of lattice oxygen and adsorbed oxygen has a great impact on catalytic performance. It is well known that the catalytic activity of VOCs, like benzene oxidation on the transition metal oxides proceeds through Mars–van Krevelen mechanism involving lattice oxygen via a redox cycle [10]. In other words, we deduce that O_{latt} is the main active oxygen species and is responsible for the high catalytic activity of $Cu_{0.5}Co_{2.5}Al$-MMO in the complete oxidation of benzene [13]. Busca suggested that lattice oxygen involved high propane catalytic total oxidation activity for a Co_3O_4 catalyst [47]. Also, there are other reported that the surface O_{ads} is the most active oxygen and is highly active during the oxidation reaction because of its higher mobility [40].

3.4. Temperature-programmed reduction

In order to check the redox properties of the series of $Cu_xCo_{3-x}Al$-MMO catalysts, H_2-TPR of all the catalysts were carried out and shown in Fig. 9. Cu_3Al-MMO sample exhibits a doublet with

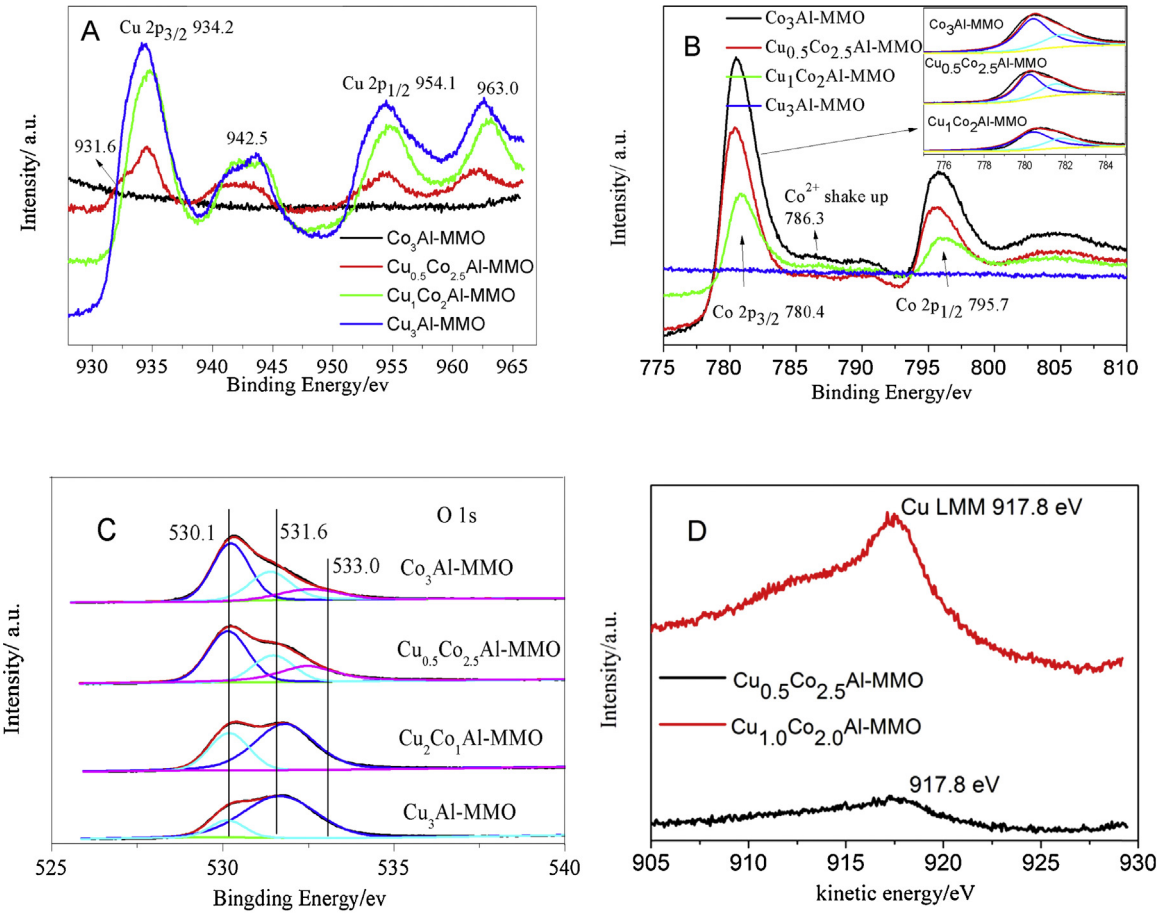

Fig. 8. XPS spectra of (A) Cu 2p, (B) Co 2p and (C) O 1s of the Co_3Al-MMO, $Cu_{0.5}Co_{2.5}Al$-MMO, Cu_2Co_1Al-MMO and Cu_3Al-MMO sample. (D) XAES spectra of Cu LMM in $Cu_{0.5}Co_{2.5}Al$-MMO and Cu_1Co_2Al-MMO samples.

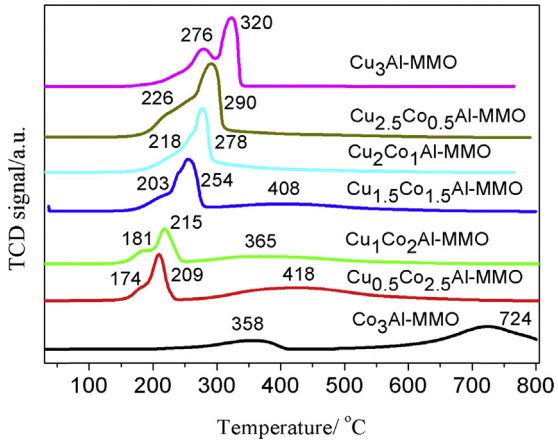

Fig. 9. Temperature-programmed reduction profiles of $Cu_xCo_{3-x}Al$-MMO catalysts.

the maximum rate of H_2 consumption for the reduction of the CuO phase occurring at *ca.* 276 and 320 °C, distinguishing from the pure CuO with one peak at 320 °C, which may be due to the existence of Cu^{2+} ions in two slightly different chemical environments, the dispersed CuO or Cu^{2+} in amorphous Al_2O_3 [49]. It can be clearly seen that the two peaks of the reduction of the CuO shift gradually toward lower temperature from 226, 290 °C for $Cu_{0.5}Co_{2.5}Al$-MMO to 174, 209 °C for $Cu_{2.5}Co_{0.5}Al$-MMO, implying that the enhanced substitution of Co^{2+} in the $Cu_xCo_{3-x}Al$-MMO catalysts framework favours the reducibility of Cu^{2+}. H_2 consumption due to the reduction of Co in Co_3O_4 spinel on the high temperature at 358 °C is very weak for Co_3Al-MMO sample. It should be noticed that the peak position was a little change to high temperature from 358 to 408 °C up to $Cu_{1.5}Co_{1.5}Al$-MMO. The Co reduction peak is not discernable with further decreasing of Co content. The results generally indicate that the reducibility of Co is diminished to some extent with increasing Cu content in the sample. The peak around 724 °C for the reduction of Co species in the Al-containing Co_3O_4 spinel is recorded only in the Co_3Al-MMO sample. In brief, while the reducibility of Cu species is enhanced with increasing cobalt content or the reducibility of Co species is diminished with increasing copper content. This result strongly reveals the existence of a synergetic interaction between copper and cobalt species, which was believed to be responsible for the catalytic activity.

3.5. *The structure and catalytic performance of the monolithic $Cu_xCo_{3-x}Al$-MMO film catalyst*

Monolithic catalysts have recently attracted much attention owing to their advantages of sufficient exposure of active sites, especially metal monolithic catalysts are good at heat conduction, comparable with the mixed oxides powder catalysts for slow internal diffusion in the industrial application. In this part, the monolithic CuCoAl-MMO film catalyst was further obtained from the calcination of the in situ growth of the CuCoAl-LDH precursor on aluminum substrates. For the LDH film precursor (Fig. 10A), a series of reflections are observed at 2θ of 11.6°, 23.2°, 34.8°and 60.1°, which can be attributed to the (0 0 3), (0 0 6), (0 0 9) and (1 1 0) plane of an LDH phase, respectively. The LDH film precursors crystallized

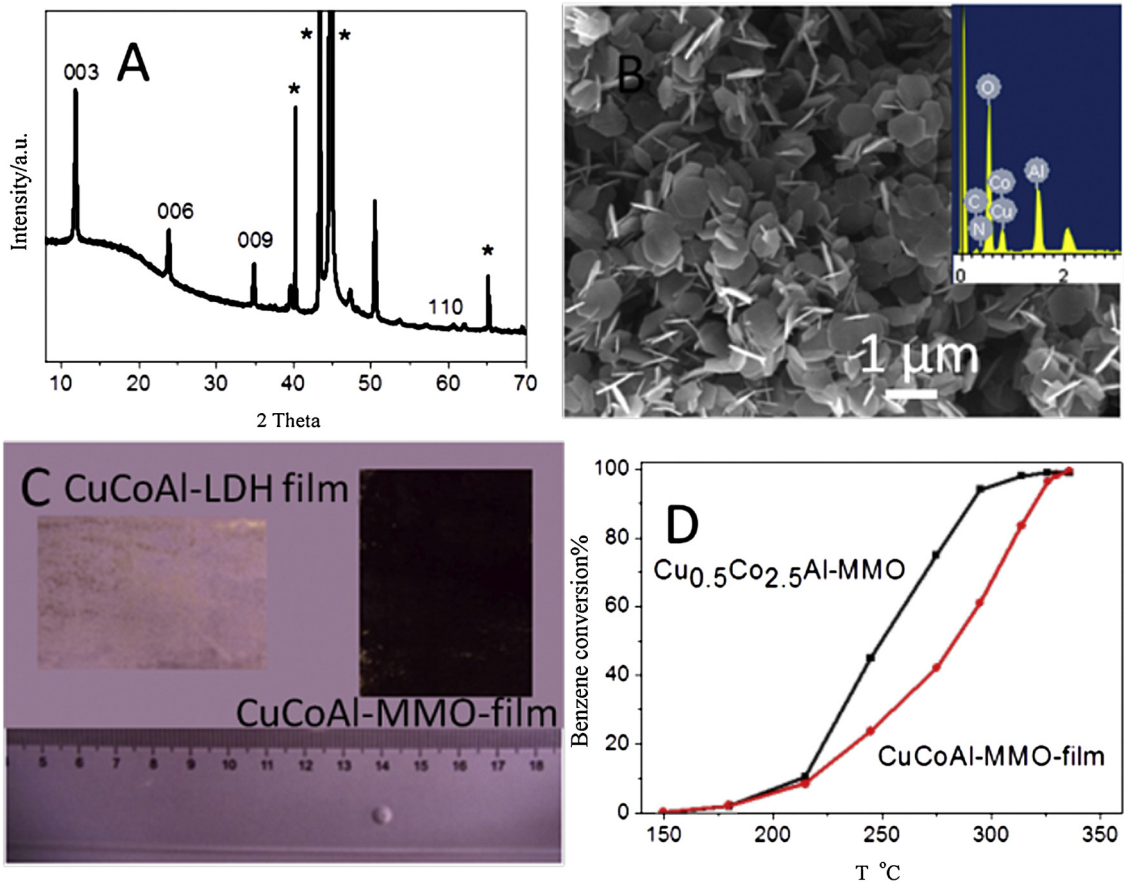

Fig. 10. (A) XRD pattern and (B) SEM images of the CuCoAl-LDH film precursor on the Al substrate (* represent the Al substrate). The inset in B show its corresponding EDX view. (C) The photograph of the monolithic CuCoAl-LDH film and CuCoAl-MMO film catalyst on the Al substrate. (D) The comparison of the benzene conversion over CuCoAl-MMO film and $Cu_{0.5}Co_{2.5}$Al-MMO powder catalyst.

as thin curved platelets with *ab* plane nearly perpendicular orientation to the support [50] (Fig. 10B). The morphology remained preserved after heating the LDH film at 400 °C, when CuO and spinel-like Co_3O_4 mixed oxides were formed (not shown here). The LDH film on Al substrate photographed by a camera turns to black color from dark pink color after calcination shown in Fig. 10C. The catalytic activity of the CuCoAl-MMO film was a little reduced for benzene conversion with T90 at 315 °C compared with the corresponding powdered catalyst $Cu_{0.5}Co_{2.5}$Al-MMO with T90 at 290 °C evaluated in Fig. 10D, which may be due to the little incorporation of Cu with the atom ratio of Cu:Co = 1:10 detected from SEM-EDX. The structural and functional superiority of the CuCoAl-MMO film catalyst makes it an exciting efficient candidate in benzene oxidation system.

4. Conclusions

In summary, a series of dispersed and porous Cu_xCo_{3-x}Al-MMO powder and monolithic film catalysts were fabricated via the LDH precursor approach, which display excellent catalytic behavior towards benzene catalytic oxidation. The structural properties and catalytic activity are seriously dependent on the relative content of the Cu:Co. Cu_xCo_{3-x}Al-MMO samples contain CuO and spinel-like Co_3O_4 mixed oxides. Compared with the single oxide, the incorporation Cu into Co_3Al-MMO resulted in decreased specific surface areas and increased pore sizes. The reducibility of Cu^{2+} species of the CuO was enhanced with increasing Co content while a reverse effect is noted for the reducibility of Co with increasing Cu content. The $Cu_{0.5}Co_{2.5}$Al-MMO catalyst shows the most active, which may be due to the larger surface area, smaller pore size, low temperature reducibility and a larger ratio of lattice oxygen to adsorption oxygen derived from the synergistic effect detected by BET, TPR and XPS. The existence of a sort of Cu–Co synergistic interaction probably originated by the intimate contact and by the good interdispersion of the oxide phases formed through the calcination of LDH precursors.

Acknowledgments

This research described above was supported by the strategic project of science and technology of Chinese Academy of Sciences (No. XDB05050000), the 863 Hi-tech Research and Development Program of China (Grant No. 2012AA062702; No. 2013AA031801) and the National Natural Science Foundation of China (No. 21401200; No. 51272253).

References

[1] A.M. Carrillo, J.G. Carriazo, Appl. Catal. B: Environ. 164 (2015) 443–452.
[2] S. Scire, L.F. Liotta, Appl. Catal. B: Environ. 125 (2012) 222–246.
[3] M. Piumetti, D. Fino, N. Russo, Appl. Catal. B: Environ. 163 (2015) 277–287.
[4] Z.-Y. Tian, T. Chafik, M. Assebban, S. Harti, N. Bahlawane, P.M. Kouotou, K. Kohse-Hoeinghaus, Appl. Energy 107 (2013) 149–156.
[5] M. Takeuchi, M. Hidaka, M. Anpo, J. Hazard. Mater. 237–238 (2012) 133–139.
[6] T. Garcia, S. Agouram, J.F. Sánchez-Royo, R. Murillo, A.M. Mastral, A. Aranda, I. Vázquez, A. Dejoz, B. Solsona, Appl. Catal. A: Gen. 386 (2010) 16–27.
[7] F.J. Varela-Gandía, Á. Berenguer-Murcia, D. Lozano-Castelló, D. Cazorla-Amorós, D.R. Sellick, S.H. Taylor, Appl. Catal. B: Environ. 129 (2013) 98–105.
[8] J. Lu, B. Fu, M.C. Kung, G. Xiao, J.W. Elam, H.H. Kung, P.C. Stair, Science 335 (2012) 1205–1208.

[9] S. Pitkaaho, L. Matejova, K. Jiratova, S. Ojala, R.L. Keiski, Appl. Catal. B: Environ. 126 (2012) 215–224.
[10] E.W. McFarland, H. Metiu, Chem. Rev. 113 (2013) 4391–4427.
[11] M. Alifanti, M. Florea, V.I. Pârvulescu, Appl. Catal. B: Environ. 70 (2007) 400–405.
[12] T. Barakat, V. Idakiev, R. Cousin, G.-S. Shao, Z.-Y. Yuan, T. Tabakova, S. Siffert, Appl. Catal. B: Environ. 146 (2014) 138–146.
[13] Z. Wang, G. Shen, J. Li, H. Liu, Q. Wang, Y. Chen, Appl. Catal. B: Environ. 138 (2013) 253–259.
[14] C. Li, J. Zhou, W. Gao, J. Zhao, J. Liu, Y. Zhao, M. Wei, D.G. Evans, X. Duan, J. Mater. Chem. A 1 (2013) 5370–5376.
[15] C. Zhang, C. Wang, W. Zhan, Y. Guo, Y. Guo, G. Lu, A. Baylet, A. Giroir-Fendler, Appl. Catal. B: Environ. 129 (2013) 509–516.
[16] G.S. Pozan, J. Hazard. Mater. 221–222 (2012) 124–130.
[17] S. Li, J. Lu, M. Wei, D.G. Evans, X. Duan, Adv. Funct. Mater. 20 (2010) 2848–2856.
[18] S. Li, J. Lu, J. Xu, S. Dang, D.G. Evans, X. Duan, J. Mater. Chem. 20 (2010) 9718–9725.
[19] S. He, Z. An, M. Wei, D.G. Evans, X. Duan, Chem. Commun. 49 (2013) 5912–5920.
[20] W. Gao, C. Li, H. Chen, M. Wu, S. He, M. Wei, D.G. Evans, X. Duan, Green Chem. 16 (2014) 1560–1568.
[21] F. Kovanda, K. Jiratova, J. Ludvikova, H. Raabova, Appl. Catal. A: Gen. 464 (2013) 181–190.
[22] L. Obalova, K. Jiratova, F. Kovanda, K. Pacultova, Z. Lacny, Z. Mikulova, Appl. Catal. B: Environ. 60 (2005) 289–297.
[23] F. Kovanda, T. Rojka, J. Dobesova, V. Machovic, P. Bezdicka, L. Obalova, K. Jiratova, T. Grygar, J. Solid State Chem. 179 (2006) 812–823.
[24] K. Jiratova, J. Mikulova, J. Klempa, T. Grygar, Z. Bastl, F. Kovanda, Appl. Catal. A: Gen. 361 (2009) 106–116.
[25] F. Kovanda, K. Jiratova, Appl. Clay Sci. 53 (2011) 305–316.
[26] V. Rives, A. Dubey, S. Kannan, Phys. Chem. Chem. Phys. 3 (2001) 4826–4836.
[27] K. Parida, L. Mohapatra, N. Baliarsingh, J. Phys. Chem. C 116 (2012) 22417–22424.
[28] S. Fleutot, J.-C. Dupin, G. Renaudinb, H. Martineza, Phys. Chem. Chem. Phys. 13 (2011) 17564–17578.
[29] S. Britto, S. Joseph, P.V. Kamath, J. Chem. Sci. 122 (2010) 751–756.
[30] M.Q. Zhao, Q.Z.W. Zhang, J.Q. Huang, Y.H. Zhang, D.S. Su, F. Wei, J. Am. Chem. Soc. 132 (2010) 14739–14741.
[31] L. He, Y.Q. Huang, A.Q. Wang, X.D. Wang, X.W. Chen, J.J. Delgado, T. Zhang, Angew. Chem. Int. Ed. 51 (2012) 6191–6194.
[32] S. He, S.T. Zhang, J. Lu, Y.F. Zhao, J. Ma, M. Wei, D.G. Evans, X. Duan, Chem. Commun. 47 (2011) 10797–10799.
[33] L. Zou, F. Li, X. Xiang, D.G. Evans, X. Duan, Chem. Mater. 18 (2006) 5852–5859.
[34] W.T. Reichle, S.Y. Kang, D.S. Everhardt, J. Catal. 101 (1986) 352–359.
[35] S.F. Zuo, F.J. Liu, J. Tong, C.Z. Qi, Appl. Catal. A: Gen. 467 (2013) 1–6.
[36] C.Y. Lu, H.H. Tseng, M.Y. Wey, L.Y. Liu, J.H. Kuo, K.H. Chuang, Fuel 88 (2009) 340–347.
[37] S.S. Hong, G.H. Lee, G.D. Lee, Korean J. Chem. Eng. 20 (2003) 440–444.
[38] S.F. Zuo, Q.Q. Huang, J. Li, R.X. Zhou, Appl. Catal. B: Environ. 91 (2009) 204–209.
[39] X. Li, L. Wang, Q. Xia, Z. Liu, Z. Li, Catal. Commun. 14 (2011) 15–19.
[40] W. Tang, X. Wu, S. Li, X. Shan, G. Liu, Y. Chen, Appl. Catal. B: Environ. 162 (2015) 110–121.
[41] J.J. Spivey, Ind. Eng. Chem. Res. 26 (1987) 2165–2180.
[42] R.M. Freire, F.F. de Sousa, A.L. Pinheiro, E. Longhinotti, J.M. Filho, A.C. Oliveira, P. de, T.C. Freire, A.P. Ayala, A.C. Oliveira, Appl. Catal. A: Gen. 359 (2009) 165–179.
[43] W. Gao, Y. Zhao, J. Liu, Q. Huang, S. He, C. Li, J. Zhao, M. Wei, Catal. Sci. Technol. 3 (2013) 1324–1332.
[44] S. Poulston, P.M. Parlett, P. Stone, M. Bowker, Surf. Interface Anal. 24 (1996) 811–820.
[45] Y. Yamada, K. Yano, Q. Xu, S. Fukuzumi, J. Phys. Chem. C 114 (2010) 16456–16462.
[46] L. Fu, Z. Liu, Y. Liu, B. Han, P. Hu, L. Cao, D. Zhu, Adv. Mater. 17 (2005) 217–221.
[47] T. Garcia, S. Agouram, J.F. Sanchez-Royo, R. Murillo, A. Maria Mastral, A. Aranda, I. Vazquez, A. Dejoz, B. Solsona, Appl. Catal. A: Gen. 386 (2010) 16–27.
[48] Y. Xia, H. Dai, L. Zhang, J. Deng, H. He, C.T. Au, Appl. Catal. B: Environ. 100 (2010) 229–237.
[49] S. Velu, K. Suzuki, S. Hashimoto, N. Satoh, F. Ohashi, S. Tomura, J. Mater. Chem. 11 (2001) 2049–2060.
[50] X.X. Guo, F.Z. Zhang, S.L. Xu, D.G. Evans, X. Duan, Chem. Commun. 44 (2009) 6836–6838.